DINAME 2019 - Proceedings of the XV International Symposium on Dynamic Problems of Mechanics,
M.A. Savi, T.G. Ritto and W.M. Bessa (Editors), ABCM, Buzios, RJ, Brazil, March 10th to 15th, 2019

Considerations about modal coupling and modal interaction for nonlinear vibrations analysis of cylindrical panels

Wanclaine Almeida Vaz da Silva and Frederico Martins Alves da Silva

School of Civil Engineering- Federal University of Goiás. Av. Universitária, nº 1488-St. Universitário. CEP 74605-200, Goiânia-Brazil.

Keywords: Cylindrical panel, Modal coupling, Modal interaction, Free Vibrations.

INTRODUCTION

Cylindrical panels are circular sectors of the cylindrical shells and they are described by the theory of the slender shells. Despite a simple geometry, the slenderness of this element makes it susceptible to loss of stability and excessive vibrations when subjected to static and dynamic loads, which can lead the structure to collapse. For these reasons, efforts should be employed to understand the nonlinear phenomena that occur in them. Among the non-linear phenomena, there is the modal coupling that is an inherent phenomenon of the stability theory of structures and this appears due to the geometric nonlinearities. Another phenomenon is the modal interaction that occurs when different modes of buckling or vibration provide the same critical load or natural frequency (Del Prado, 2001; Gonçalves and Del Prado, 2004; Rodrigues et al., 2013). Therefore, this study aims to contribute to the understanding of the phenomena: modal coupling and modal interaction in simply supported cylindrical panels. To consider both phenomena, the transverse displacement field was deduced from a perturbation technique (Gonçalves, 1987; Gonçalves and Batista, 1988; Silva et al., 2011).

MATHEMATICAL FORMULATION

For the mathematical formulation, Donnell's non-linear theory for shallow shell is used, considering that the cylindrical panel is simply supported with a time-dependent transversal load. The material is assumed as linear, homogeneous and isotropic. Thus, the transversal equilibrium equation is given by Eq. (1) as a function of Airy's stress function, Eq. (2).

$$\begin{aligned}&\rho h\ddot{w}+D(w_{,xxxx}+\frac{2}{R^2}w_{,\theta\theta xx}+\frac{1}{R^4}w_{x\theta\theta\theta})-f_{,\theta\theta}(w_{,x}+w_{0,x})_{,x}+R\,f_{,xx}\\&-f_{,xx}(w_{,\theta}+w_{0,\theta})_{,\theta}-2\,f_{x\theta}(w_{,\theta x}+w_{0,\theta x})-p(t)+\beta_1\dot{w}=0\end{aligned} \tag{1}$$

$$\frac{\nabla^4 f(x,\theta)}{E\,h}=\frac{1}{R^4}(w_{,x\theta}{}^2-w_{,xx}w_{,\theta\theta}+R\,w_{,xx}+2\,w_{,x\theta}w_{0,x\theta}-w_{,xx}w_{0,\theta\theta}-w_{,\theta\theta}w_{0,xx}) \tag{2}$$

where D is the flexural stiffness, R is the radius of curvature, h is the thickness' cylindrical panel, ρ is the density, $p(t)$ is the time-dependent transversal load distributed along the domain, β_1 is the parameter of viscous damping and E is the Young's modulus. This problem considers an initial geometrical imperfection, given by w_0.

NUMERICAL RESULTS

In order to determine the geometries that have modal interaction, linear free vibrations results are obtained for a simply supported panel. For this, it is used the classical vibration modes for the transverse displacement field for a simply supported cylindrical panel. Thus, an algebraic expression of the natural frequency is deduced depending on the geometric, stiffness and mechanical parameters and the number of axial half-wave, m, and number of circumferential half-wave, n. Table 1 presents the chosen geometries that they provoke different types of internal resonance between two different vibration modes (1:1 and 1:2) while Table 2 shows the chosen geometry that generates internal resonance between three different vibration modes (1:1:2).

The transversal displacement field, that will be used to obtain the nonlinear frequency-amplitude (backbones) relation, is obtained applying a perturbation technique (Gonçalves, 1987; Gonçalves and Batista, 1988; Silva et al., 2011; Rodrigues et al., 2014). To start the perturbation procedure, it is necessary to consider a seed solution, which in this work, it has the sum of linear vibration modes that present the same natural frequency (Tables 1 and 2). Thus, the perturbation procedure gives the correct modal solution that considers the modal coupling and modal interaction for a

simply-supported cylindrical panel. The used modal solutions for each internal resonance cases, that are presented in Tables 1 and 2, are shown in Tables 3-5. It is important to notice that the model W1 of each case of internal resonance is the used seed solution to start the perturbation procedure to obtain transversal displacement field.

Table 1 - Geometries with modal interaction between two modes. (*R*=1m, *L*=0.1m, *h*=0.001m, *E*=206x10^9 N/m² and ρ=7800kg/m³).

Axial half-wave	Θ (radian)	Internal resonance	Circumferential half-wave	Natural frequency (Hz)
***m*=1**	0.1658	1:1	***n*=1**	686.293
***m*=1**			***n*=2**	686.293
***m*=1**	0.0707	1:2	***n*=1**	778.721
***m*=2**			***n*=1**	1557.442

Table 2 – Geometry with modal interaction between three modes. (*R*=1m, Θ=0.169 rad, *h*=0.001m, *E*=206x10^9 N/m² and ρ=7800kg/m³).

Axial half-wave	L (m)	Internal resonance	Circumferential half-wave	Natural frequency (Hz)
***m*=1**	0.091	1:1:2	***n*=1**	741.876
***m*=1**			***n*=2**	741.876
***m*=2**			***n*=1**	1483.752

Table 3 - Modal solutions for transversal field displacements considering the 1:1 internal resonance case

Model	Modal solutions
W1	$\sin\left(\frac{\pi x}{L}\right)\left[A1_{11}(t)\,\sin\left(\frac{\pi\theta}{\Theta}\right)+A2_{11}(t)\,\sin\left(\frac{2\pi\theta}{\Theta}\right)\right]$
W2	$W_1+\sin\left(\frac{\pi x}{L}\right)\left[+A1_{13}(t)\,\sin\left(\frac{3\pi\theta}{\Theta}\right)+A2_{13}(t)\sin\left(\frac{6\pi\theta}{\Theta}\right)\right]$
W3	$W_2+\sin\left(\frac{\pi x}{L}\right)\left[\,A3_{11}(t)\,\mathrm{sen}\left(\frac{4\pi\theta}{\Theta}\right)+A5_{11}(t)\sin\left(\frac{5\pi\theta}{\Theta}\right)+A6_{11}(t)\,\sin\left(\frac{3\pi\theta}{\Theta}\right)\right]$
W4	$W_1+A7_{22}(t)\left[\frac{3}{4}-\cos\left(\frac{2\pi x}{L}\right)+\frac{1}{4}\cos\left(\frac{4\pi x}{L}\right)\right]\left[\frac{3}{4}-\cos\left(\frac{2\pi\theta}{\Theta}\right)+\frac{1}{4}\cos\left(\frac{4\pi\theta}{\Theta}\right)\right]$
W5	$W_4+A8_{22}(t)\left[\frac{3}{4}-\cos\left(\frac{2\pi x}{L}\right)+\frac{1}{4}\cos\left(\frac{4\pi x}{L}\right)\right]\left[\frac{3}{4}-\cos\left(\frac{4\pi\theta}{\Theta}\right)+\frac{1}{4}\cos\left(\frac{8\pi\theta}{\Theta}\right)\right]$
W6	$W_2+A7_{22}(t)\left[\frac{3}{4}-\cos\left(\frac{2\pi x}{L}\right)+\frac{1}{4}\cos\left(\frac{4\pi x}{L}\right)\right]\left[\frac{3}{4}-\cos\left(\frac{2\pi\theta}{\Theta}\right)+\frac{1}{4}\cos\left(\frac{4\pi\theta}{\Theta}\right)\right]$ $+A8_{22}(t)\left[\frac{3}{4}-\cos\left(\frac{2\pi x}{L}\right)+\frac{1}{4}\cos\left(\frac{4\pi x}{L}\right)\right]\left[\frac{3}{4}-\cos\left(\frac{4\pi\theta}{\Theta}\right)+\frac{1}{4}\cos\left(\frac{8\pi\theta}{\Theta}\right)\right]$
W7	$W_3+A7_{22}(t)\left[\frac{3}{4}-\cos\left(\frac{2\pi x}{L}\right)+\frac{1}{4}\cos\left(\frac{4\pi x}{L}\right)\right]\left[\frac{3}{4}-\cos\left(\frac{2\pi\theta}{\Theta}\right)+\frac{1}{4}\cos\left(\frac{4\pi\theta}{\Theta}\right)\right]$ $+A8_{22}(t)\left[\frac{3}{4}-\cos\left(\frac{2\pi x}{L}\right)+\frac{1}{4}\cos\left(\frac{4\pi x}{L}\right)\right]\left[\frac{3}{4}-\cos\left(\frac{4\pi\theta}{\Theta}\right)+\frac{1}{4}\cos\left(\frac{8\pi\theta}{\Theta}\right)\right]$

Table 4- Modal solutions for transversal field displacements considering the 1:2 internal resonance case.

Model	Modal solutions
W1	$\sin\left(\frac{\pi\theta}{\Theta}\right)\left[A1_{11}(t)\sin\left(\frac{\pi x}{L}\right)+A2_{11}(t)\sin\left(\frac{2\pi x}{L}\right)\right]$
W2	$W_2+\sin\left(\frac{\pi\theta}{\Theta}\right)\left[A1_{13}(t)\sin\left(\frac{3\pi x}{L}\right)+A2_{13}(t)\sin\left(\frac{6\pi x}{L}\right)\right]$
W3	$W_2+\sin\left(\frac{\pi\theta}{\Theta}\right)[\ A3_{11}(t)\sin\left(\frac{2\pi x}{L}+\frac{2\pi x}{L}\right)+A4_{11}(t)\sin\left(\frac{2\pi x}{L}-\frac{2\pi x}{L}\right)$ $+A5_{11}(t)\sin\left(\frac{4\pi x}{L}+\frac{\pi x}{L}\right)+A6_{11}(t)\ \sin\left(\frac{4\pi x}{L}-\frac{\pi x}{L}\right)\ ]$
W4	$W_1+A7_{22}(t)\left[\frac{3}{4}-\cos\left(\frac{2\pi x}{L}\right)+\frac{1}{4}\cos\left(\frac{4\pi x}{L}\right)\right]\left[\frac{3}{4}-\cos\left(\frac{2\pi\theta}{\Theta}\right)+\frac{1}{4}\cos\left(\frac{4\pi\theta}{\Theta}\right)\right]$
W5	$W_4+A8_{22}(t)\left[\frac{3}{4}-\cos\left(\frac{2\pi x}{L}\right)+\frac{1}{4}\cos\left(\frac{4\pi x}{L}\right)\right]\left[\frac{3}{4}-\cos\left(\frac{4\pi\theta}{\Theta}\right)+\frac{1}{4}\cos\left(\frac{8\pi\theta}{\Theta}\right)\right]$
W6	$W_2+A7_{22}(t)\left[\frac{3}{4}-\cos\left(\frac{2\pi x}{L}\right)+\frac{1}{4}\cos\left(\frac{4\pi x}{L}\right)\right]\left[\frac{3}{4}-\cos\left(\frac{2\pi\theta}{\Theta}\right)+\frac{1}{4}\cos\left(\frac{4\pi\theta}{\Theta}\right)\right]$ $+A8_{22}(t)\left[\frac{3}{4}-\cos\left(\frac{2\pi x}{L}\right)+\frac{1}{4}\cos\left(\frac{4\pi x}{L}\right)\right]\left[\frac{3}{4}-\cos\left(\frac{4\pi\theta}{\Theta}\right)+\frac{1}{4}\cos\left(\frac{8\pi\theta}{\Theta}\right)\right]$
W7	$W_3+A7_{22}(t)\left[\frac{3}{4}-\cos\left(\frac{2\pi x}{L}\right)+\frac{1}{4}\cos\left(\frac{4\pi x}{L}\right)\right]\left[\frac{3}{4}-\cos\left(\frac{2\pi\theta}{\Theta}\right)+\frac{1}{4}\cos\left(\frac{4\pi\theta}{\Theta}\right)\right]$ $+A8_{22}(t)\left[\frac{3}{4}-\cos\left(\frac{2\pi x}{L}\right)+\frac{1}{4}\cos\left(\frac{4\pi x}{L}\right)\right]\left[\frac{3}{4}-\cos\left(\frac{4\pi\theta}{\Theta}\right)+\frac{1}{4}\cos\left(\frac{8\pi\theta}{\Theta}\right)\right]$

To obtain the Airy's stress function, Eq. (2), the showed modal expansions of Tables 3-5 are substituted into Eq. (2) and solved it analytically. The obtained stress function and the chosen modal expansion are substituted into equilibrium equation, Eq. (1), and discretized by standard Galerkin method, obtaining a discrete reduced order model of perfect cylindrical panel. The non-linear frequency-amplitude relation are determined applying the shooting method (Mattos, 1984) in the obtained set of second-order differential equation which that are shown in Figure 1.

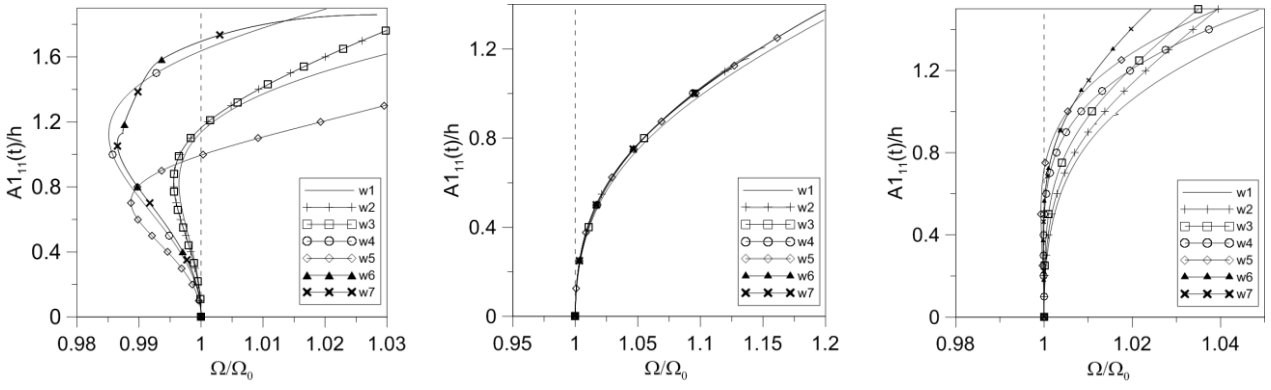

(a) 1:1 internal resonance (b) 1:2 internal resonance (c) 1:1:2 internal resonance

Figure 1- Frequency-amplitude ratio for (a) 1:1, (b) 1:2 and (c) 1:1:2 internal resonance cases for a perfect cylindrical panel

It is possible to note from Fig. 1 the influence of the considered modal solution for transversal displacement field on the nonlinear frequency-amplitude relation for each analyzed internal resonance case. The considered reduced order models (W_i, i=1…7) in Tables 3-5 are obtained expanding the general transversal solution given by the perturbation

procedure. In general way, we consider only terms that contain sine function, or cosine functions, to sum the seed solution of each internal resonance cases (W_1 in Tables 3-5). In Fig. 1(a), Models W_1, W_2 and W_3 generate the same frequency-amplitude relation up to panel's thickness amplitude while Models W_4, W_5, W_6 and W_7 (presence of cosine functions) display more softening behavior nonlinearity than Models W_1, W_2 and W_3. From Figs. 1(b)-1(c), the considered reduced order models with sine functions, or cosine functions, give the same frequency-amplitude relation being different only to high amplitude vibrations.

From previous work, the forced nonlinear response of cylindrical panels will be strongly affected with the presence of cosine functions (Silva et al., 2016) and in this work the modal solution *W6* that it is able to consider the modal interaction effects and it is able to ensure the convergence up to thickness vibration amplitudes. For the analysis of the influence of an initial geometric imperfection on the nonlinear behavior of cylindrical panels with internal resonance, w_0, is considered as:

$$w_0 = C_1 \sin\left(\frac{\pi x}{L}\right)\sin\left(\frac{\pi\theta}{\Theta}\right) \tag{3}$$

where C_1 is the amplitude of geometrical imperfection.

Table 5- Modal solutions for transversal field displacements considering the 1:1:2 internal resonance case

Model	Modal expansion
W1	$\sin\left(\frac{\pi x}{L}\right)\left[A1_{11}(t)\sin\left(\frac{\pi\theta}{\Theta}\right)+A2_{11}(t)\sin\left(\frac{2\pi\theta}{\Theta}\right)\right]+A3_{11}(t)\sin\left(\frac{2\pi x}{L}\right)\sin\left(\frac{\pi\theta}{\Theta}\right)$
W2	$W_1+\sin\left(\frac{\pi x}{L}\right)\left[A1_{13}(t)\sin\left(\frac{3\pi\theta}{\Theta}\right)+A2_{13}(t)\sin\left(\frac{6\pi\theta}{\Theta}\right)\right]+A3_{13}(t)\sin\left(\frac{2\pi x}{L}\right)\sin\left(\frac{3\pi\theta}{\Theta}\right)$
W3	$W_2+\sin\left(\frac{\pi\theta}{\Theta}\right)\left[A4_{11}(t)\sin\left(\frac{3\pi x}{L}\right)+A5_{11}(t)\sin\left(\frac{5\pi x}{L}\right)\right]$ $+\sin\left(\frac{2\pi\theta}{\Theta}\right)\left[A6_{11}(t)\sin\left(\frac{3\pi x}{L}\right)+A7_{11}(t)\sin\left(\frac{5\pi x}{L}\right)\right]$
W4	$W_1+A28_{22}(t)\left[\frac{3}{4}-\cos\left(\frac{2\pi x}{L}\right)+\frac{1}{4}\cos\left(\frac{4\pi x}{L}\right)\right]\left[\frac{3}{4}-\cos\left(\frac{2\pi\theta}{\Theta}\right)+\frac{1}{4}\cos\left(\frac{4\pi\theta}{\Theta}\right)\right]$ $+A29_{22}(t)\left[\frac{3}{4}-\cos\left(\frac{2\pi x}{L}\right)+\frac{1}{4}\cos\left(\frac{4\pi x}{L}\right)\right]\left[\frac{3}{4}-\cos\left(\frac{4\pi\theta}{\Theta}\right)+\frac{1}{4}\cos\left(\frac{8\pi\theta}{\Theta}\right)\right]$
W5	$W_4+A30_{22}(t)\left[\frac{3}{4}-\cos\left(\frac{4\pi x}{L}\right)+\frac{1}{4}\cos\left(\frac{8\pi x}{L}\right)\right]\left[\frac{3}{4}-\cos\left(\frac{2\pi\theta}{\Theta}\right)+\frac{1}{4}\cos\left(\frac{4\pi\theta}{\Theta}\right)\right]$
W6	$W_2+A28_{22}(t)\left[\frac{3}{4}-\cos\left(\frac{2\pi x}{L}\right)+\frac{1}{4}\cos\left(\frac{4\pi x}{L}\right)\right]\left[\frac{3}{4}-\cos\left(\frac{2\pi\theta}{\Theta}\right)+\frac{1}{4}\cos\left(\frac{4\pi\theta}{\Theta}\right)\right]$ $+A29_{22}(t)\left[\frac{3}{4}-\cos\left(\frac{2\pi x}{L}\right)+\frac{1}{4}\cos\left(\frac{4\pi x}{L}\right)\right]\left[\frac{3}{4}-\cos\left(\frac{4\pi\theta}{\Theta}\right)+\frac{1}{4}\cos\left(\frac{8\pi\theta}{\Theta}\right)\right]$ $+A30_{22}(t)\left[\frac{3}{4}-\cos\left(\frac{4\pi x}{L}\right)+\frac{1}{4}\cos\left(\frac{8\pi x}{L}\right)\right]\left[\frac{3}{4}-\cos\left(\frac{2\pi\theta}{\Theta}\right)+\frac{1}{4}\cos\left(\frac{4\pi\theta}{\Theta}\right)\right]$
W7	$W_3+A28_{22}(t)\left[\frac{3}{4}-\cos\left(\frac{2\pi x}{L}\right)+\frac{1}{4}\cos\left(\frac{4\pi x}{L}\right)\right]\left[\frac{3}{4}-\cos\left(\frac{2\pi\theta}{\Theta}\right)+\frac{1}{4}\cos\left(\frac{4\pi\theta}{\Theta}\right)\right]$ $+A29_{22}(t)\left[\frac{3}{4}-\cos\left(\frac{2\pi x}{L}\right)+\frac{1}{4}\cos\left(\frac{4\pi x}{L}\right)\right]\left[\frac{3}{4}-\cos\left(\frac{4\pi\theta}{\Theta}\right)+\frac{1}{4}\cos\left(\frac{8\pi\theta}{\Theta}\right)\right]$ $+A30_{22}(t)\left[\frac{3}{4}-\cos\left(\frac{4\pi x}{L}\right)+\frac{1}{4}\cos\left(\frac{8\pi x}{L}\right)\right]\left[\frac{3}{4}-\cos\left(\frac{2\pi\theta}{\Theta}\right)+\frac{1}{4}\cos\left(\frac{4\pi\theta}{\Theta}\right)\right]$

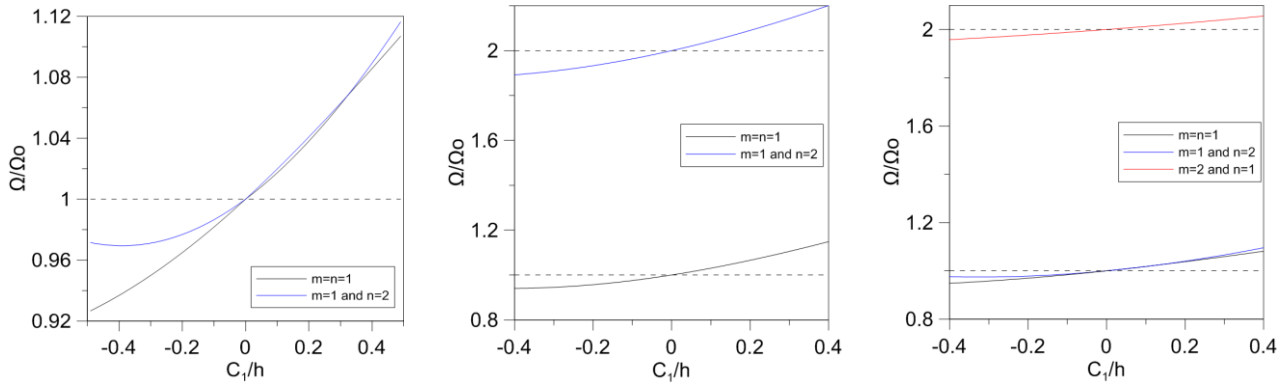

(a) 1:1 internal resonance (b) 1:2 internal resonance (c) 1:1:2 internal resonance

Figure 2- Variation of the natural frequency as a function of C_1/h for (a) 1:1, (b) 1:2 and (c) 1:1:2 internal resonances.

Initially, the influence of amplitude of an initial geometrical imperfection on the natural frequency of cylindrical panel is investigated, as shown in Fig. 2, for each internal resonance case. Fig. 2 shows the variation of the natural frequency, normalized with respect to the natural frequency of perfect cylindrical panel, of each vibration modes with the amplitude of initial geometrical imperfection. From Fig. 2(a), it is shows that positive values of C_1/h increase the natural frequency for both modes of vibration and their values are quite closer them, maintaining in certain aspects the 1:1 internal resonance. On the other hand, negative values of C_1/h, decrease the natural frequency of each vibration mode and destroying the 1:1 internal resonance. Already Figs. 2(b) and 2(c) indicate that the natural frequency increase for positive values of C_1/h and decrease to negative values of C_1/h for all vibration modes that generate the internal resonance and the ratio between the natural frequency of vibration modes remains, in certain aspects, closer than same ratio of a perfect cylindrical panel, maintaining the internal resonances for all analyzed amplitudes' imperfection.

From the system of ordinary second-order nonlinear differential equations for an imperfect cylindrical panel, an analysis of nonlinear free vibrations was conducted. Figure 3 shows the frequency- amplitude relations for the internal resonance cases investigated in this work, considering an initial geometrical with different amplitudes, C_1/h, where the continuous lines (—) represent the first linear mode of vibration and the symbol (-●-) represents the second linear mode of vibration that are the used seed solution of perturbation procedure.

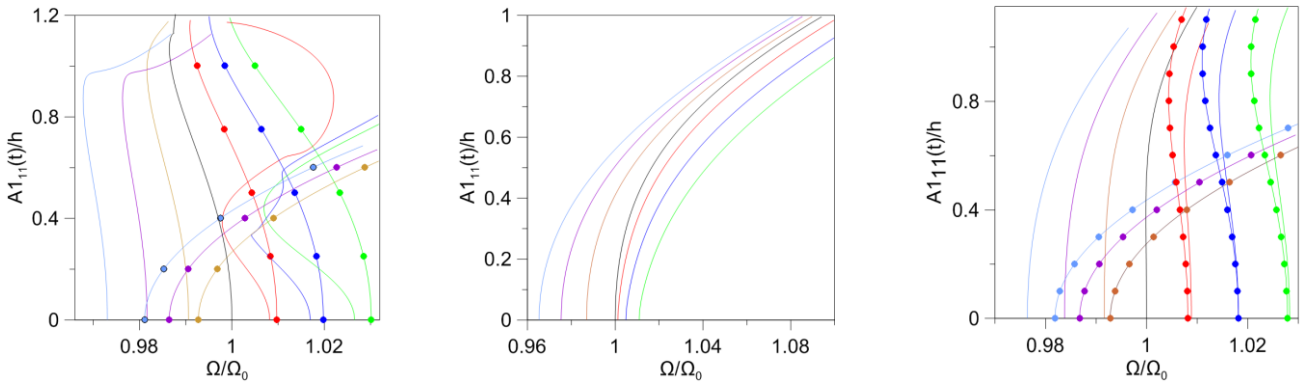

(a) 1:1 internal resonance (b)1:2 internal resonance c) 1:1:2 internal resonance

Figure 3 - Frequency amplitude relation for (a) 1:1, (b) 1:2 and (c) 1:1:2 internal resonance, considering different geometrical imperfection's amplitude.

(--- C_1/h = 0.0; --- C_1/h = 0.05; — C_1/h = 0.10; — C_1/h = 0.15; --- C_1/h = -0.05, --- C_1/h =-0.10, — C_1/h =-0.15)

Figure 3 shows the frequency-amplitude relation for an imperfect cylindrical panel with different types of internal resonance. Firstly, in Fig. 3(a), that it is related with 1:1 internal resonance, a pair of frequency-amplitude relation for each imperfection's amplitude, related with each linear vibration modes, is observed in the region of first natural frequency. The nonlinear behavior of imperfect cylindrical panel is a softening behavior followed by a hardening frequency-amplitude relation for all cases of positive values for imperfection's amplitude, C_1/h. Already for negative values of imperfection's amplitude, the first vibration mode (m=n=1) displays initially a softening nonlinear frequency amplitude relation while the second vibration mode (m=1 and n=2) displays only hardening nonlinear frequency

amplitude relation. This coexisting pair of frequency-amplitude relation, that occurs due to the presence of initial geometric imperfections, can change strongly the main characteristics of nonlinear resonance curves of cylindrical panel.

Figure 3(b) shows the frequency-amplitude relation for the case of internal resonance of type 1:2. In this case, the frequency region analyzed has only the backbone curve for the first vibration mode (m=n=1), and the nonlinear behavior is with hardening effects. As shown in Fig. 2(b) and observed in Fig. 3(b), for positive values of imperfection's amplitude the backbone curves move to the left due to increasing of system's stiffness while for negative values the frequency-amplitude relation curves move to the right because of decreasing of system's stiffness. Already in Fig. 3(c), the frequency-amplitude relation for the case of an imperfect cylindrical panel with 1:1:2 internal resonance appears in pair in the region of the first natural frequency, as already observed in Fig. 3(a), but for positive values of imperfection's amplitude both linear modes (m=n=1) and (m=1 and n=2) display a backbone curve with softening type nonlinearity while for negative values of imperfection the same modes present a frequency-amplitude relation with hardening type nonlinearity. From Fig. 3, it is observed that the presence of imperfection can change the nonlinearity characteristics' system modifying the global stiffness' cylindrical panel.

To evaluate the nonlinear forced vibrations in simply supported cylindrical panels, a lateral load is applied in the panel domain in the form of the fundamental mode of vibration which is given by Eq. (4) where pl is the amplitude of lateral load and w is the frequency of excitation. The viscous damping is considered as indicated in Eq. (5), where η_1 is the viscous damping coefficient.

$$p(t) = pl \sin\left(\frac{n\pi\theta}{\Theta}\right)\sin\left(\frac{m\pi x}{L}\right)\cos(\Omega t) \tag{4}$$

$$\beta_1 = 2\eta_1 \rho h \Omega_0 \tag{5}$$

where Ω and Ω_0 are, respectively, the frequency of excitation and the first natural frequency of perfect cylindrical panel.

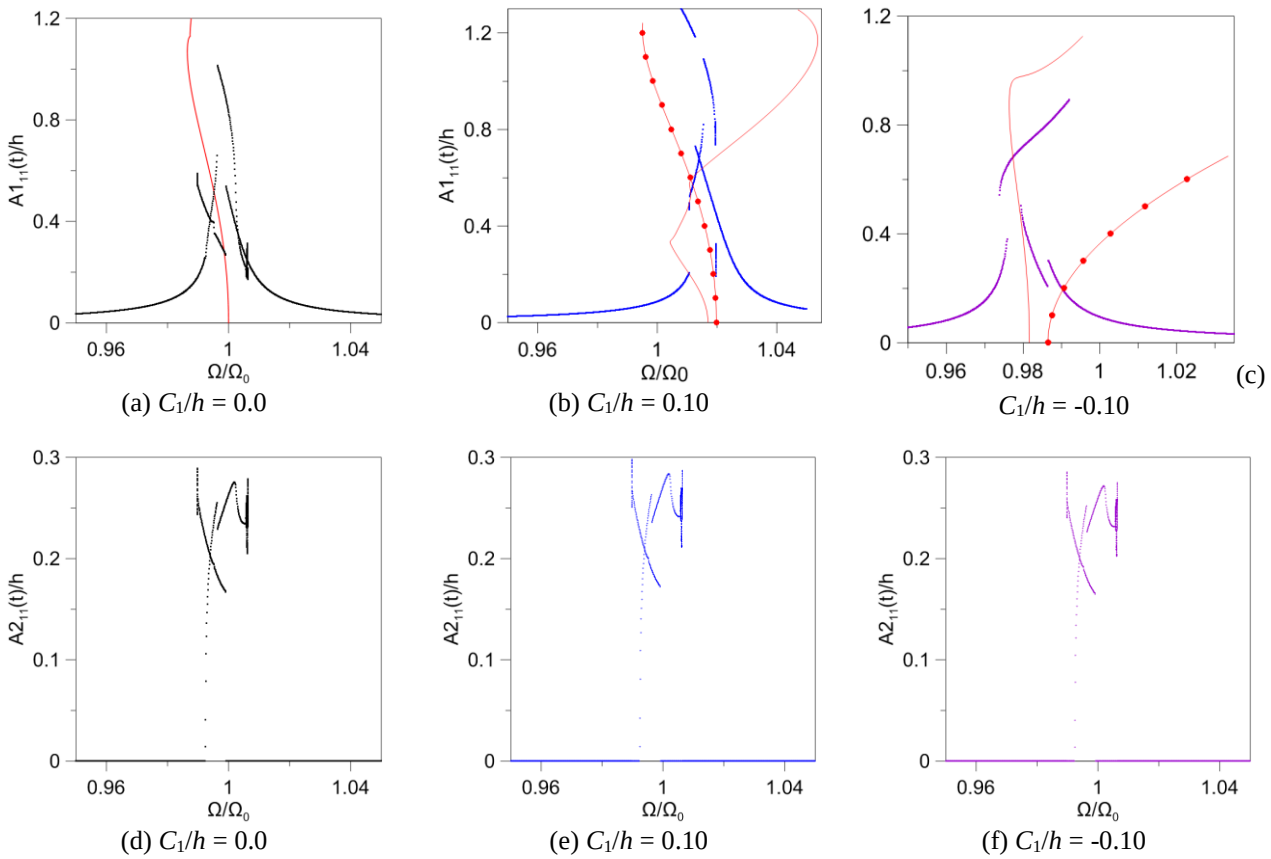

(a) C_1/h = 0.0 (b) C_1/h = 0.10 (c) C_1/h = -0.10

(d) C_1/h = 0.0 (e) C_1/h = 0.10 (f) C_1/h = -0.10

Figure 4- Resonance curve for 1:1 internal resonance.*pl* = 1 kN/m², η_1 = 0.001.

The obtained resonance curves are shown in Figs. 4-6 for each analyzed internal resonance and they were obtained by a brute force method that maps the maximum amplitude of the permanent time-response, plotting this maximum amplitude of vibration versus the frequency of excitation. For each internal resonance case studied, there are the

obtained numerical resonance curves for the perfect cylindrical panel (---- C_1/h = 0.0), the imperfect cylindrical panel with positive amplitude's imperfection (---- C_1/h = 0.10) and the imperfect cylindrical panel with negative amplitude's imperfection (---- C_1/h =-0.10).

In Fig. 4 it is shown, as expected, that the resonance curves of the first vibration mode follow the backbone curves of the cylindrical panel. It is also observed that the geometric imperfection, presented in Figs. 4(b) and 4(c), modifies the dynamic stability scenario, creating new stable paths. About the sign of imperfection, it is observed that the vibration amplitude decreases in the case of negative values of C_1/h and it increases in case of positive values of C_1/h. As shown in Figs. 4(d)-4(f), the lateral load, described by Eq. (4), can excite the second vibration mode in the main resonance region independently of the sign of amplitude's imperfection due to internal resonance that remains in the presence of imperfection, as seen in Fig. 2(a) and 3(a).

From Figs. 5(a) to 5(c), it is noted that the resonance curves of the first vibration mode for imperfect cylindrical panel, Figs. 5(b) and 5(c), do not modify its stability and dynamical jumps when compared with the resonance curve of a perfect cylindrical panel with 1:2 internal resonance, Fig. 5(a). For all resonance curves presented in Fig. 5 there is a typical saddle-node bifurcation, independently of amplitude's imperfection, and the nonlinear behavior is maintained. As expected from Figs. 2(b) and 3(b), the presence of imperfections changes only the natural frequency, moving the backbone curves to left (or right) due to increasing (or decreasing) of system's stiffness. It is important to notice that in this case of internal resonance 1:2, the lateral pressure, that excites the vibration mode (m=n=1), in the presence of an initial geometrical imperfection that displays the same shape of vibration mode (m=n=1), does not excite the second vibration mode (m=1 and n=2), as shown in Figs. 5(d)-5(f).

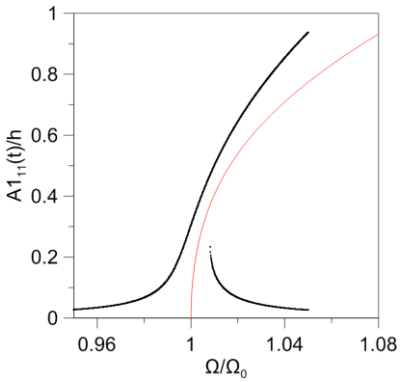

(a) C_1/h = 0.0

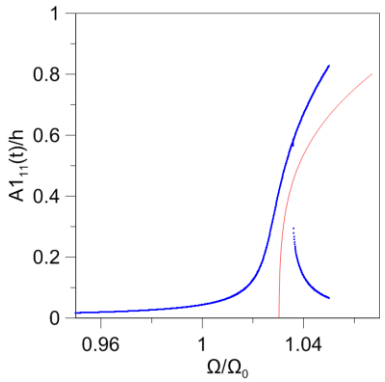

(b) C_1/h = 0.10

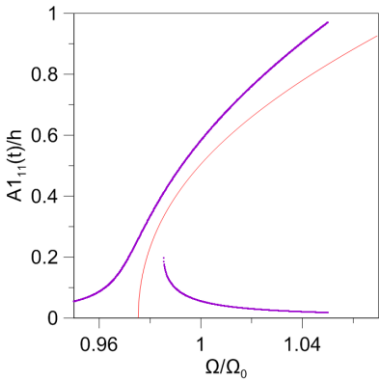

(c) C_1/h = -0.10

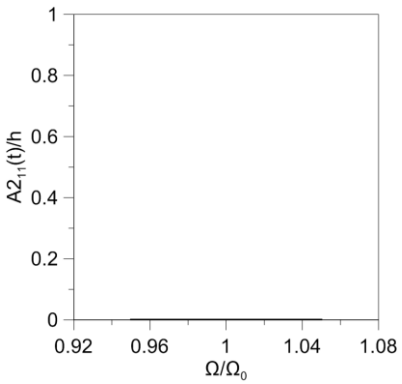

(d) C_1/h = 0.0

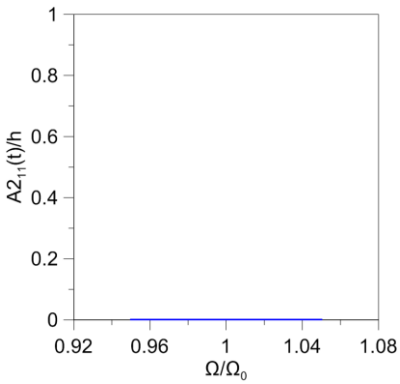

(e) C_1/h = 0.10

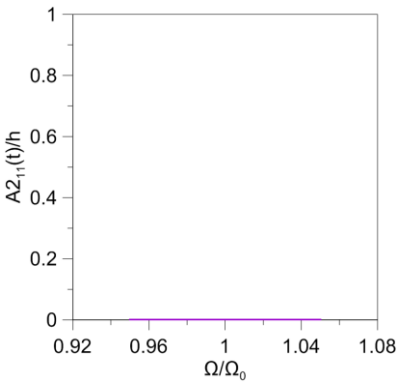

(f) C_1/h = -0.10

Figure 5 Resonance curve for 1:2 internal resonance. pl = 1 kN/m², η_1 = 0.001.

Finally, in Fig. 6 is presented the resonance curves for a cylindrical panel with 1:1:2 internal resonance considering different values of imperfection's amplitude. From Fig. 6(a) to 6(c), it is observed that the resonance curves of the first vibration mode follow the behavior of its backbone curves. The geometric imperfection's amplitude depicted by C_1/h changes the dynamic stability of the system, the shape of the resonance curve and the vibration amplitude for both positive values and for negative values of C_1/h. The nonlinear forced response of cylindrical panel is more complex (dynamical jumps and bifurcation scenario) for positive values of C_1/h than negative values. From Figs. 6(d) to 6(f), it is important to note that the participation of the second vibration mode is strongly dependent of the sign's amplitude's imperfection. For the considered cases of Figs. 6(d) (perfect cylindrical panel) and Fig. 6(e) (imperfect cylindrical panel with positive value for amplitude's imperfection), the lateral load can excite the second mode of vibration. On the other hand, Fig. 6(f) (imperfect cylindrical panel with positive value for amplitude's imperfection), the lateral load does not

excite the second mode of vibration, indicating that geometric imperfection contributes to the participation of the second vibration mode.

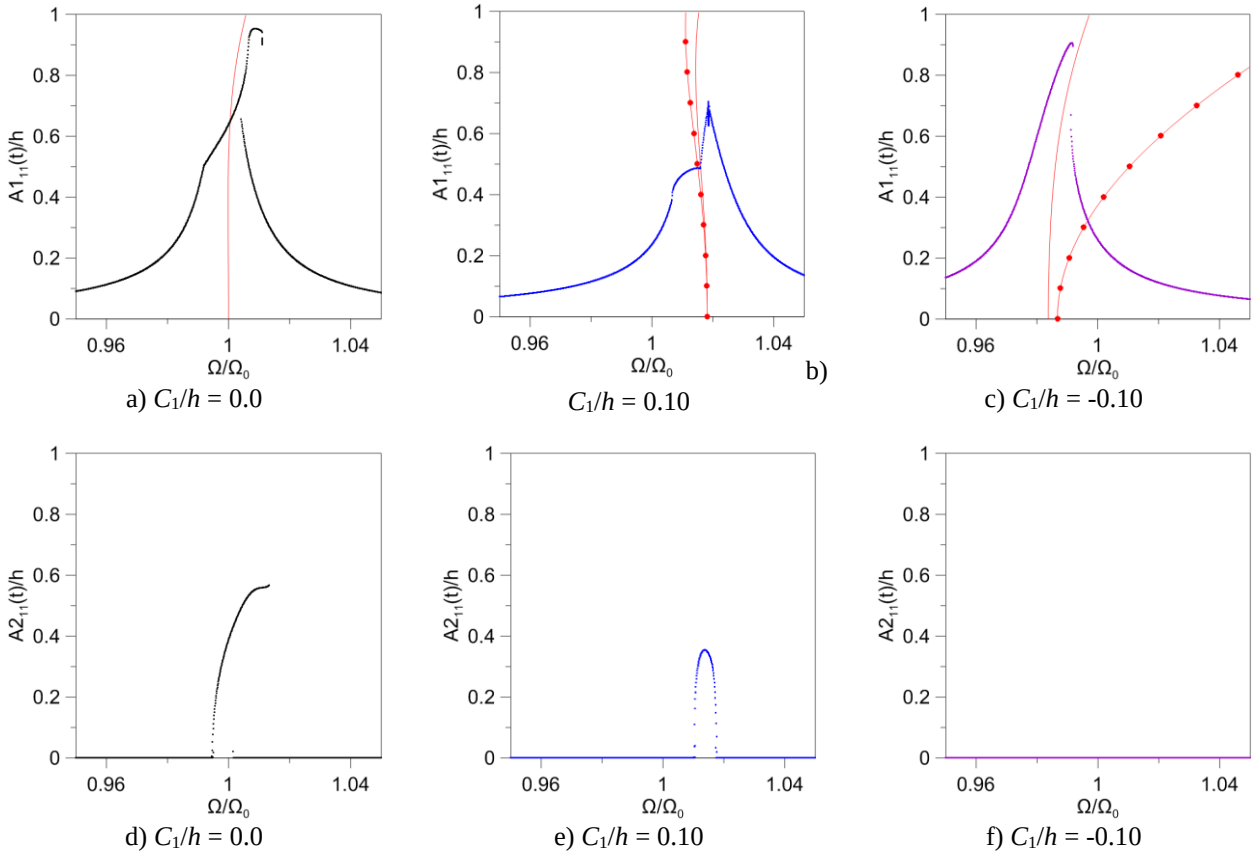

a) C_1/h = 0.0 b) C_1/h = 0.10 c) C_1/h = -0.10

d) C_1/h = 0.0 e) C_1/h = 0.10 f) C_1/h = -0.10

Figure 6 Resonance curve for 1:1:2 internal resonance. *pl* = 1.5 kN/m², η_1 = 0.001.

CONCLUDING REMARKS

This paper investigates the influence of the modal coupling and modal interaction on the nonlinear free vibrations of cylindrical panels. It is important to notice that a new consistent modal solution, that take into account the modal interaction between two, or three, different vibration modes, were developed by the authors. Important modifications in the nonlinear free vibration can be observed. It was verified in free vibration analysis that the geometric imperfection in the fundamental mode shape increases the stiffness of the cylindrical panel for positive values of amplitudes' imperfections and decreases the stiffness of the cylindrical panel for negative values of amplitudes' imperfection. Other analysis to be noticed is that the modal interaction can be destroyed with increasing intensity in modulus of amplitudes' imperfection. It is observed that the forced vibrations of cylindrical panel with an initial geometrical imperfection in the shape of fundamental mode modifies the vibration amplitudes, the dynamic stability and bifurcation scenario of the resonance curves for the cases of internal resonance 1:1 and 1:1:2 due to interaction that occurs between the linear modes. On the other hand, the chosen shape of geometrical imperfection does not exhibit any effect on the resonance curve of a cylindrical panel with 1:2 internal resonance, excited by a lateral load in the shape of fundamental vibration mode. This work is on progress and other geometrical imperfection's shape must be considered to analyze the nonlinear resonance curves.

ACKNOWLEDGEMENTS

This work was made possible by the support of the Brazilian Ministry of Education, CAPES, CNPq and FAPEG.

REFERENCES

Del Prado, Z. J. G. N, 2001, "Acoplamento e interação modal na instabilidade dinâmica de cascas cilíndricas". Tese (Doutorado em Engenharia Civil) - Pontifícia Universidade Católica do Rio de Janeiro. Rio de Janeiro, p. 193.

Gonçalves, P. B, 1987, "Interação dinâmica não-linear entre fluido e cascas delgadas". Tese de Doutorado - COPPE, Universidade Federal do Rio de Janeiro. Rio de Janeiro, p. 317. 1987.

Gonçalves, P. B., Batista, R. C., 1988, "Non-linear vibration analysis of fluid-filled cylindrical shells". Journal of Sound and Vibration, Vol. 127, pp. 133-143.

Gonçalves, P. B., Del Prado, Z. J. G N, 2004, "Effect of non-linear modal interaction on the dynamic instability of axially excited cylindrical shells". Computers and Structures, Vol. 82, pp. 2621-2634.

Mattos, H. S. C, 1984, "Método do tiro para resolução de estruturas unidimensionais". Rio de Janeiro. Dissertação de Mestrado – DEM, Pontifícia Universidade Católica do Rio de Janeiro.

Rodrigues, L., Silva, F. M. A., Gonçalves, P. B., Del Prado, Z. J. G. N., 2013, "Effects of modal coupling on the dynamics of parametrically and directly excited cylindrical shells". Thin-walled structures, Vol. 81, pp. 210-224.

Rodrigues, L., Gonçalves, P. B., Silva, F. M. A., 2017, "Internal resonances in a transversally excited imperfect circular cylindrical shell". Procedia Engineering, Vol. 199, pp. 838-843.

Silva, F. M. A., Gonçalves, P. B., Del Prado, Z. J. G. N., 2011, "An alternative procedure for the non-linear vibration analysis of fluid-filled cylindrical shells". Nonlinear Dynamics, Vol. 66, pp. 303-333.

Silva, F. M. A., Sattler, H. A. R., Gonçalves, P. B., Del Prado, Z. J. G. N., 2016, "Influence of Modal Coupling on the Nonlinear Vibration of Simply Supported Cylindrical Panels". Applied Mechanics and Materials, Vol. 849, pp. 106-118.